

# Diagnosing Altermagnetic Phases through Quantum Oscillations

Zhi-Xia Li,<sup>1</sup> Xiangang Wan,<sup>1</sup> and Wei Chen<sup>1,\*</sup>

<sup>1</sup>National Laboratory of Solid State Microstructures, School of Physics,  
and Collaborative Innovation Center of Advanced Microstructures, Nanjing University, Nanjing 210093, China  
(Dated: June 7, 2024)

The recently delimited altermagnetic phase is characterized by zero net magnetization but momentum-dependent collinear spin-splitting. To explore the intriguing physical effects and potential applications of altermagnets, it is essential to analyze their Fermi surface properties, encompassing both configurations and spin textures. Here, we conduct a Fermiology study on metallic altermagnets and demonstrate that the collinear spin-split features of their Fermi surfaces can be clearly revealed through quantum oscillation measurements. By introducing a transverse Zeeman field to remove the spin-degenerate lines in the momentum space, the Fermi surface undergoes a Lifshitz transition, giving rise to spin-flipped cyclotron motion between orbits with opposite spins. Accordingly, the Lifshitz-Onsager quantization yields two sets of Landau levels, leading to frequency splitting of the Shubnikov-de Haas oscillations in conductivity. In the presence of spin-orbit coupling, the Zeeman field causes two separate cyclotron orbits to merge at the Lifshitz transition point before splitting again. This results in the two original frequencies discontinuously changing into a single frequency equal to their sum. Our work unveils a unique and universal signature of altermagnetic Fermi surfaces that can be probed through quantum oscillation measurements.

*Introduction.*—The investigation of magnetic systems has long been an active branch of condensed matter physics. Among various magnetically ordered phases, the collinear quantum magnets are usually divided into two phases, ferromagnetism and antiferromagnetism [1]. Recently, a new type of collinear magnetic phase dubbed altermagnetism has been proposed based on spin group theory and is attracting increasing attention in condensed matter physics [2–4]. Distinct from ferromagnetism and conventional antiferromagnetism, such materials exhibit large momentum-dependent spin splitting in their bands and zero net magnetization at the same time, which are induced by nonrelativistic spin and crystal rotation symmetry [2–5]. The spin-dependent Fermi surfaces of altermagnets exhibit the  $d$ -,  $g$ -, or  $i$ -wave symmetries, which lead to many intriguing physical properties, such as spin current [6–8], anomalous Hall effect [9], crystal magneto-optical Kerr effect [10] and giant magnetoresistance [5] that cannot occur in conventional antiferromagnets. Altermagnets are predicted to have various potential applications, including spintronics [11–13], correlated states of matter [3], superconductivity [14, 15], *etc.*

Hundreds of material candidates have been predicted to be altermagnetic [16], including three-dimensional compounds such as MnTe, RuO<sub>2</sub>, and La<sub>2</sub>CuO<sub>4</sub> [3, 17–19], and two-dimensional monolayer RuF<sub>4</sub> with the  $d$ -wave altermagnetic symmetry [20]. Very recently, the altermagnetic lifting of Kramers spin degeneracy has been observed in RuO<sub>2</sub> and MnTe (MnTe<sub>2</sub>) by angle-resolved photoemission spectroscopy (ARPES) or spin-ARPES [21–24], demonstrating the  $d$ -wave spin pattern in RuO<sub>2</sub> [22]. Meanwhile, the muon spin rotation and relaxation experiment on RuO<sub>2</sub> has reported the absence of magnetic order [25, 26], casting doubt on the diagnosis of altermagnetic phase. Consequently, further measure-

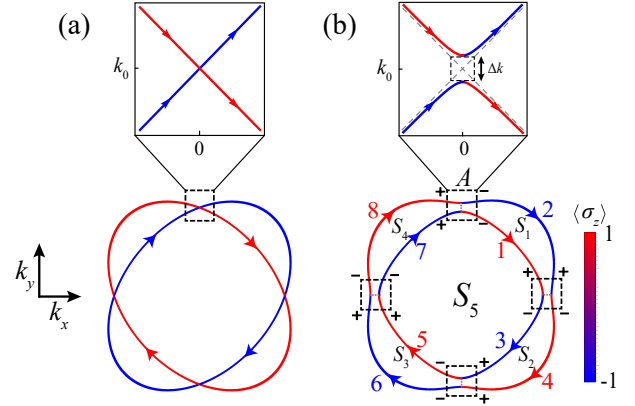


FIG. 1. Schematic illustration of cyclotron motion along Fermi surfaces (a) with and (b) without the in-plane Zeeman field. The upper panels are zoom-in images at the transition regions denoted by the dashed boxes. The average value  $\langle \sigma_z \rangle$  is measured by the color bar. The numbers in (b) label the line segments and  $S_1, \dots, S_5$  denote the areas of respective regions encircled by them. The incoming and outgoing states are labeled by + and -, respectively.

ments, such as quantum oscillations, are necessary to ascertain the nature of altermagnets. Moreover, to understand the intriguing physical effects of the altermagnets and explore their potential applications, it is essential to analyze the geometric and spin configurations of altermagnetic Fermi surfaces.

In this Letter, we study quantum oscillations in metallic altermagnets to uncover the distinctive properties of their Fermi surfaces. By imposing an in-plane Zeeman field to remove spin degeneracy along specific lines in the momentum space which then causes a Lifshitz transition of the Fermi surface, the altermagnets can be diagnosed through the frequency transitions of Shubnikov-de

Haas oscillations in conductivity. Specifically, as the Zeeman field increases, the cyclotron orbits change from two identical orbits for both spin polarizations to two reconstructed ones with spin hybridization. Then, the Lifshitz-Onsager quantization [27] along these cyclotron orbits results in the splitting of Landau levels, which is manifested as the Zeeman-field induced frequency splitting of the Shubnikov-de Haas oscillations. When spin-orbit coupling (SOC) exists whose effect cannot be neglected in certain material candidates, a  $\pi$  Berry phase is accumulated along two pristine cyclotron orbits. In such a regime, a Zeeman field can drive two semiclassical orbits to merge together, leading to an discontinuously change of the oscillation frequency from two components to a single one. Our results can be generally applied to various material candidates of altermagnets, thus providing an effective and universal approach for its identification.

*Spin-flipped cyclotron motion.*—To be specific, we consider a 2D  $d$ -wave metallic altermagnet with a Zeeman field along the  $x$ -direction, which can be described by the Hamiltonian as

$$H(\mathbf{k}) = a(k_x^2 + k_y^2) + Jk_x k_y \sigma_z + \Delta \sigma_x, \quad (1)$$

where  $\mathbf{k} = (k_x, k_y)$  is the momentum,  $\sigma_{x,y,z}$  are the spin Pauli matrices,  $a$  and  $J$  parameterize the kinetic term and the  $d$ -wave exchange interaction, respectively.  $\Delta = \mu_B B_x g^*/2$  is the Zeeman energy splitting with  $B_x$  the Zeeman field and  $g^*$  the Landé  $g$  factor. The corresponding eigenenergies are

$$E_{\pm}(k) = a(k_x^2 + k_y^2) \pm \sqrt{J^2 k_x^2 k_y^2 + \Delta^2}. \quad (2)$$

In the absence of a Zeeman field ( $\Delta = 0$ ), the Fermi surface is composed of two intersecting ellipses corresponding to two opposite spins [Fig. 1(a)]; A finite Zeeman field hybridizes the two spin bands and accordingly, the Fermi surface undergoes a Lifshitz transition characterized by a momentum separation  $\Delta k$  at the originally degenerate points [Fig. 1(b)].

As a perpendicular magnetic field  $B$  in the  $z$  direction is applied, electrons are driven to move along equienergy contours (labeled by  $O$ ). In the absence of tunneling between different orbits, the eigenenergies are selected by the following quantization condition

$$S(O) = 2\pi l^{-2}(n + \gamma), \quad n = 0, 1, 2, \dots, \quad (3)$$

where  $S$  is the area encircled by the cyclotron orbits in the momentum space,  $l = \sqrt{\hbar/eB}$  is the magnetic length, and  $\gamma = 1/2$  is the Maslov index [28].

More generally, a magnetic breakdown may occur between the outer and inner Fermi contours in Fig. 1(b) [29], which leads to more complicated quantization rules compared with Eq. (3). To analyze the magnetic breakdown, we adopt the Landau gauge for the vector potential as  $\mathbf{A} = (0, Bx, 0)$  and make the substitution  $k_y \rightarrow k_y + Bx$  in Eq. (1), where  $\hbar = 1, e = 1$

is set for simplicity. In the momentum representation, the coordinate operator reads  $x \rightarrow i\partial_{k_x}$ . Quantum tunneling may occur in the breakdown regions marked with black dashed squares in Fig. 1(b). Given the symmetry of the Fermi surface, it is sufficient to analyze one specific region A and then combine the results of four regions. In region A,  $k_x \simeq 0, k_y \simeq k_0 = \sqrt{E_F/a}$  with  $E_F$  the Fermi energy, and the Hamiltonian (2) can be expanded at  $(k_x, k_y) = (0, k_0)$  to the linear order of momentum as

$$\mathcal{H}(\mathbf{k}) = ak_0(2k_y - k_0) + Jk_0 k_x \sigma_z + \Delta \sigma_x, \quad (4)$$

which gives two hyperbola segments of Fermi surface as shown in the upper panel of Fig. 1(b). By interpreting  $k_x \equiv t$  as time, the problem of magnetic breakdown can be mapped to the model of Landau-Zener tunneling [30]. A direct calculation yields the tunnel probability  $Z = \exp(-\frac{\pi}{B} \frac{\Delta^2}{2aJk_0^2})$  [31], which will be used to determine the quantization conditions.

*Quantization conditions and Landau levels.*—We regard  $k_y$  as a parameter and solve the state evolution in region A in the  $k_x \equiv t$  representation. Consider an electron entering region A from  $k_x < 0$  and exiting to  $k_x > 0$ ; see the upper panel of Fig. 1(b). A straightforward derivation yields the scattering matrix  $\mathcal{S}$  that connects the incident and outgoing waves as [30, 32]

$$\begin{pmatrix} c_2^- \\ c_1^- \end{pmatrix} = \mathcal{S} \begin{pmatrix} c_8^+ \\ c_7^+ \end{pmatrix}, \mathcal{S} = \begin{pmatrix} \sqrt{1-Z}e^{-i\omega} & -\sqrt{Z} \\ \sqrt{Z} & \sqrt{1-Z}e^{i\omega} \end{pmatrix}, \quad (5)$$

where the amplitudes  $(c_8^+, c_7^+)^T$  and  $(c_2^-, c_1^-)^T$  correspond to the incoming (+) and outgoing (-) states, respectively [cf. Fig. 1(b)].  $\omega$  is the so-called Stokes phase [33] which reads

$$\omega = \frac{\pi}{4} + \delta(\ln \delta - 1) + \text{Arg}[\Gamma(1 - i\delta)], \quad \delta = \frac{\Delta^2}{4BaJk_0^2}, \quad (6)$$

where  $\Gamma(\cdot)$  is the gamma function.

A full cyclotron motion constitutes four such scattering processes connected by free propagations along the line segments denoted by  $i = 1, \dots, 8$  in Fig. 1(b), in which the areas surrounded by the line segments are denoted by  $S_{1, \dots, 5}$ . Due to the  $C_4$  rotation symmetry of the orbits, the four equal areas are set to  $S_{1, \dots, 4} = S_0$ . Define  $\Theta_i$  as the phase accumulation during the free propagation along the line segment  $i$ . Since the amplitudes  $\{c_i^+, c_i^-\}$  are everywhere single-valued, we arrive at the following equation

$$\det \left\{ \prod_{j=1}^4 \left[ \mathcal{S} \begin{pmatrix} e^{i\Theta_{2j}} & 0 \\ 0 & e^{i\Theta_{2j-1}} \end{pmatrix} \right] - \mathcal{I} \right\} = 0, \quad (7)$$

where the matrix product is arranged from right to left as  $j$  increases, and  $\mathcal{I}$  is the identity matrix. For any cyclotron orbit  $O$ , the accumulated phase during free prop-

agation is given by [28]

$$\sum_{i \in O} \Theta_i = l^2 S(O) - 2\pi\gamma, \quad (8)$$

where the sum is taken over the line segments that constitute the orbit  $O$ . Solving Eq. (7) yields the quantization condition as [30]

$$\begin{aligned} \cos[l^2(S_5 + 2S_0) - 2\pi\gamma] - (1 - Z)^2 \cos(2l^2 S_0 - 4\omega) \\ + 4Z(1 - Z) \cos(l^2 S_0 - 2\omega) + Z(2 - 3Z) = 0. \end{aligned} \quad (9)$$

For an arbitrary  $Z$ , the quantized energy spectra can be obtained by inserting the explicit functions  $S_5 = S_5(E)$  and  $S_0 = S_0(E)$  of energy  $E$  into Eq. (9).

Our main focus is on the two semiclassical limits  $Z \rightarrow 1$  (magnetic breakdown regime) and  $Z \rightarrow 0$  (adiabatic regime), which correspond to scenarios with small and large Zeeman fields, respectively. In these two limits, the quantization conditions reduce to

$$\begin{aligned} Z \rightarrow 1 : S_5 + 2S_0 &= 2\pi l^{-2}(n + \gamma), \\ Z \rightarrow 0 : S_5 + 4S_0 &= 2\pi l^{-2}(n + \gamma), \text{ or } S_5 = 2\pi l^{-2}(n + \gamma), \end{aligned} \quad (10)$$

where we have considered in the second line that  $\omega \rightarrow 0$  as  $Z \rightarrow 0$ . The quantization condition for  $Z \rightarrow 1$  correspond to the two identical ellipse-shaped orbits in Fig. 1(a), which yields the spin-degenerate Landau levels  $E_n = (eB/\hbar)\sqrt{4a^2 - J^2}(n + \gamma)$ . In the  $Z \rightarrow 0$  limit, the two quantization conditions correspond to the outer and inner orbits respectively in Fig. 1(b), which give rise to two different sets of Landau levels.

To verify such observations, we numerically calculate the energy levels as a function of  $B$  in the two limits. To this end, we interpret  $x$  and  $k_x$  by the ladder operators as  $x = \sqrt{\hbar/2eB}(\pi + \pi^\dagger)$  and  $k_x = i\sqrt{eB/2\hbar}(\pi^\dagger - \pi)$ , which operate on the Landau level basis through  $\pi|n\rangle = \sqrt{n}|n-1\rangle$  and  $\pi^\dagger|n\rangle = \sqrt{n+1}|n+1\rangle$ . A proper cutoff is adopted for  $n$  in the calculation to ensure the convergence of the results. In the rest of this paper,  $k_x$  and  $x$  are set to be dimensionless and accordingly,  $a$  and  $J$  have the units of energy. The Landau levels in both limits, as a function of  $B$ , are shown in Fig. 2. Specifically, there is only one set of Landau levels with spin degeneracy in the limit  $Z \rightarrow 1$  as shown Fig. 2(a); In the opposite limit  $Z \rightarrow 0$ , two sets of Landau levels become visible in Fig. 2(b), corresponding to the quantized outer and inner orbits in Fig. 1(b). Away from the two semiclassical limits, the typical energy spectra solved by the quantization condition exhibit a quasirandom feature, which can be treated using the perturbation theory [28].

*Shubnikov-de Haas oscillations.*—The analysis of the Landau levels indicates that the main features of alternating Fermi surface can be well reflected by the evolution of the quantum oscillations as the Zeeman field varies. Here, we focus on the Shubnikov-de Haas oscillations in conductivity. As  $B$  changes, whenever the Fermi

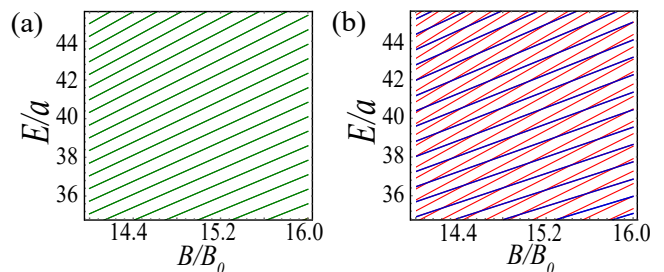


FIG. 2. Landau levels as a function of  $B$  in (a) the  $Z \rightarrow 1$  limit with  $\Delta = 0$  and  $Z \rightarrow 0$  limit with  $\Delta = 10a$ . Other parameters are  $J = 0.7a$  and  $B_0 = \hbar/(40e)$ .

level is aligned with one of the Landau levels, the density of states (DOS) reaches a maximum, leading to an oscillating behavior in resistivity. Using the linear response theory, the conductivity tensor reads [34, 35]

$$\sigma_{\mu\nu} = \frac{e^2 \hbar}{\pi V} \int dE f(E) \text{Re} \left\{ \text{Tr} \left[ \hat{v}_\mu \frac{\partial \hat{G}_E^R}{\partial E} \hat{v}_\nu (\hat{G}_E^A - \hat{G}_E^R) \right] \right\}, \quad (11)$$

where the subscripts  $\mu(\nu) = x, y$  and accordingly,  $\sigma_{xx}$  and  $\sigma_{xy}$  represent the longitudinal and Hall conductivity, respectively.  $f(E) = [e^{(E-E_F)/kT} + 1]^{-1}$  is the Fermi-Dirac distribution function,  $\hat{v}_\mu = \partial_{k_\mu} H(\mathbf{k} + \mathbf{A})$  is the velocity operator, and  $\hat{G}^{R,A} = [E - H(\mathbf{k} + \mathbf{A}) \pm i\chi]^{-1}$  are the retarded (+) and advanced (-) Green operators with  $\chi$  the level broadening. Eq. (11) is evaluated by inserting the complete Landau level basis  $\{|n\rangle\}$  and expressing the velocity operator by the ladder operators  $\pi, \pi^\dagger$ . The corresponding longitudinal resistivity is given by  $\rho_{xx} = \sigma_{xx}/(\sigma_{xx}^2 + \sigma_{xy}^2)$ . The reduced magnetoresistivity is defined as the difference between the resistivity in the presence of a magnetic field and the resistivity without a magnetic field, normalized by the latter. Specifically,  $\delta\rho_{xx}(B) = [\rho_{xx}(B) - \rho_{xx}(0)]/\rho_{xx}(0)$ .

The numerical results for  $\delta\rho_{xx}$  as a function of  $1/B$  in the two limits  $Z \rightarrow 1$  and  $Z \rightarrow 0$  are shown in Fig. 3(a) and Fig. 3(c), respectively, with Fig. 3(b) and Fig. 3(d) being their Fourier components. One can see that for  $Z \rightarrow 1$ , the oscillation of  $\delta\rho_{xx}$  consists of one main frequency component  $F_0$  and its multiples with much weaker amplitudes, corresponding to the contribution from only one set of Landau levels in Fig. 2(a). For  $Z \rightarrow 0$ , the oscillation contains two main frequency components  $F_1$  and  $F_2$ , as well as their multiples, corresponding to the two sets of Landau levels in Fig. 2(b), which is induced by the Zeeman field. To reveal the frequency transition induced by the Zeeman field, it is sufficient to calculate the DOS at the Fermi level  $E_F$ . This can be approximated using a Gaussian function with a finite broadening ( $\Sigma$ ) as

$$D(E_F, B) = \sum_n n_L \sqrt{\frac{1}{\pi \Sigma^2}} \exp \left[ -\frac{(E_F - E_n)^2}{\Sigma^2} \right], \quad (12)$$

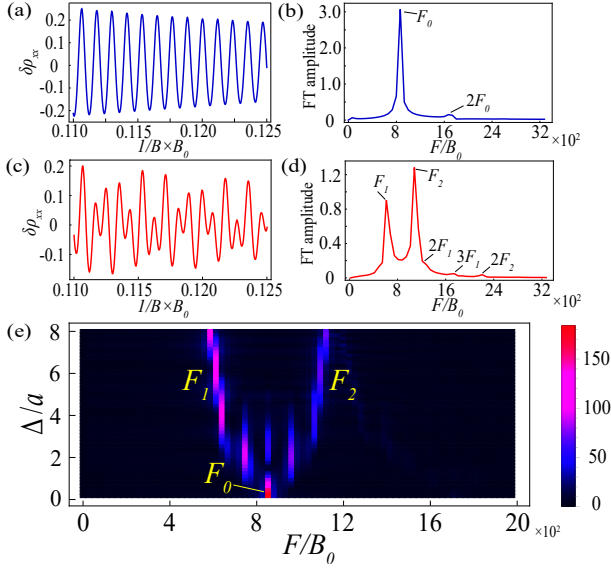


FIG. 3. The normalized longitudinal magnetoresistivity  $\delta\rho_{xx}$  as a function of  $1/B$  in the limit of (a)  $Z \rightarrow 1$  ( $\Delta = 0$ ) and (c)  $Z \rightarrow 0$  ( $\Delta = 5.6a$ ). (b) and (d) are The Fourier components of (a) and (c), respectively. (e) Fourier components of the oscillating DOS  $\delta D(E_F, B)$  as a function of  $\Delta$ . The parameters are  $J = 0.7a$ ,  $E_F = 40a$ ,  $B_0 = \hbar a/eE_F$ ,  $\Sigma = 0.2a$ ,  $\chi = 0.16a$ ,  $kT = 0.04a$ , and  $n_L/B\sqrt{\pi} = 1$ .

where  $n_L = eBL^2/\hbar\pi$  is the degeneracy of Landau levels,  $L$  is the size of the system, and  $n$  is the Landau level index. The Fourier component of the oscillating DOS,  $\delta D(E_F, B) = D(E_F, B) - D(E_F, 0)$  as a function of  $\Delta$  is shown in Fig. 3(e). In experiments, quantum oscillations are visible only when the Landau level spacing is larger than its broadening  $\Sigma$ . As one can see in Fig. 3(e), only one frequency  $F_0$  exists for  $\Delta \sim 0$ . As  $\Delta$  increases, the frequency pattern evolves and finally splits into two branches  $F_1$  and  $F_2$ . Such a frequency transition effectively manifests the collinear spin-splitting of the altermagnetic Fermi surfaces and so can serve as its fingerprint signature.

*The effect of spin-orbit coupling.*—In certain material candidates of altermagnets, the SOC effect cannot be neglected, which can be described by the whole Hamiltonian  $H(\mathbf{k}) + H_R(\mathbf{k})$  with the second term corresponding to the Rashba SOC as  $H_R(\mathbf{k}) = \lambda(k_x\sigma_y - k_y\sigma_x)$ , where  $\lambda$  is the strength of the Rashba SOC [3]. In the absence of the in-plane Zeeman term ( $\Delta = 0$ ), the SOC can still induce a petal-shaped Fermi surface similar to that in Fig. 1(b), but with a vortical spin texture, as shown in Fig. 4(a). The vortical spin winding indicates that as an electron moves along the outer or inner cyclotron orbit in Fig. 4(a), it will feel a nontrivial Berry phase  $\phi_B = \pi$  [30]. Consider the Rashba SOC is strong enough so that the magnetic breakdown can be neglected, the semiclassical quantization of the two orbits  $\alpha_1$  and  $\alpha_2$  in Fig. 4(a)

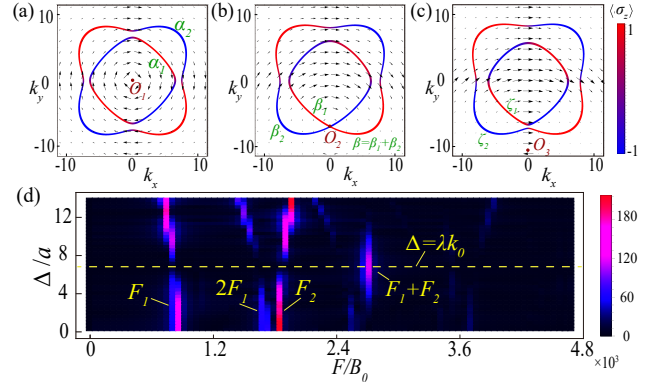


FIG. 4. (a-c) Evolution of Fermi surfaces and upper-band spin textures of altermagnets with SOC as the Zeeman field increases from (a)  $\Delta = 0$  to (b)  $\Delta = \lambda k_0 = \sqrt{48}a$  and finally to (c)  $\Delta = 11a$ . The in-plane spin textures are denoted by the arrows while its  $z$  component is represented by the color.  $O_{1,2,3}$  are the centers of the spin vortices during the evolution and  $\alpha_{1,2}, \beta_{1,2}, \beta, \zeta_{1,2}$  label the cyclotron orbits. (d) Fourier amplitudes of the oscillating DOS  $\delta D(E_F, B)$  in the presence of SOC. The critical value for the Zeeman field  $\Delta = \lambda k_0$  is marked with the yellow dashed line. The parameters are  $J = a$ ,  $\lambda = a$  and  $E_F = ak_0^2 = 48a$ ,  $B_0 = \hbar a/eE_F$ . The Landau level broadening  $\Sigma$  in (d) is set to  $0.12a$ .

becomes

$$S(\alpha_{1,2}) = 2\pi l^{-2}(n + \gamma - \phi_B/2\pi). \quad (13)$$

As the Zeeman field  $\Delta$  increases from zero, the center of the spin vortex shifts downward from the origin, following the path  $O_1 \rightarrow O_2 \rightarrow O_3$  in Figs. 4(a-c), along with the gap closing and reopening at the point  $O_2 = (0, -k_0)$ . In particular, at the Lifshitz transition point, where  $\Delta = \lambda k_0$ , the two Fermi surfaces converge at  $O_2$ , coinciding with the center of the spin vortex. Meanwhile, the tunnel probability between the outer and inner orbits at the  $O_2$  saturates with  $Z \rightarrow 1$ , indicating that the two orbits,  $\beta_1$  and  $\beta_2$ , merge into a single orbit,  $\beta = \beta_1 + \beta_2$ , as shown in Fig. 4(b). Accordingly, the quantization condition is modified into

$$S(\beta) = S(\beta_1) + S(\beta_2) = 2\pi l^{-2}(n + \gamma). \quad (14)$$

When  $\Delta > \lambda k_0$ , the two orbits separate again and the center of the vortex shifts to the outside of both Fermi contours as shown in Fig. 4(c). As a result, the Berry phase accumulated along the two semiclassical orbits  $\zeta_1$  and  $\zeta_2$  becomes zero, with the corresponding quantization condition being

$$S(\zeta_{1,2}) = 2\pi l^{-2}(n + \gamma). \quad (15)$$

We verify the above analysis again by numerically calculating the magnetic quantum oscillation of DOS with SOC using Eq. (12), and the corresponding Fourier amplitudes are shown in Fig. 4(d). As one can see, for

$\Delta \ll \lambda k_0$  and  $\Delta \gg \lambda k_0$ , there exist two main branches of frequencies  $F_1$  and  $F_2$  stemming from the contributions from both two semiclassical orbits, along with their multiples. By contrast, for  $\Delta \simeq \lambda k_0$ ,  $F_1$  and  $F_2$  disappear and instead, a visible frequency  $F_1 + F_2$  shows up, corresponding to the contribution from the combined orbit  $\beta$  in Fig 4(b) and the quantization condition (14). We conclude that in the presence of the SOC effect, the Zeeman field-induced frequency transition exhibits an enriched structure, which is another distinctive signature of altermagnets.

*Discussion.*—The experimental identification of the altermagnetic phase remains controversial at present [21, 22, 25, 26]. Therefore, additional evidence from various approaches is crucial for its diagnosis. Quantum oscillation measurements is a widely used method for characterizing the properties of the Fermi surface, including its configuration and band topology, *etc.* [32]. We have shown that by imposing a Zeeman field to lift the spin degeneracy along specific lines in momentum space, the altermagnetic spin-splitting feature can be clearly revealed by the frequency transitions in the quantum oscillations, regardless of the presence of SOC effects. To achieve this, the Landau level spacing  $(eB/\hbar)\sqrt{4a^2 - J^2}$  of altermagnets should be smaller than the typical Zeeman splitting  $\Delta$  that induces the Lifshitz transition of the Fermi surface. This requires either a high-quality sample that ensures high oscillating resolution for a small magnetic field  $B$  or a relatively large Zeeman splitting. The latter can be implemented by selecting materials with a large Landé  $g$  factor or introducing an exchange field via magnetic dopants [36]. From the inter-orbit tunneling probability  $Z = \exp(-\frac{\pi}{B} \frac{\Delta^2}{2aJk_0^2})$ , a small size  $k_0$  of the Fermi surface facilitates an efficient adjustment of the frequency transition between two tunneling limits. Although our work focuses on  $d$ -wave altermagnets, the main conclusions can be applied to other symmetries such as  $g$ - and  $i$ -wave symmetries, due to the universality of the scenario.

W.C. acknowledges the support from the National Natural Science Foundation of China under Grant No. 12074172, No. 12222406, the National Key Projects for Research and Development of China under Grant No. 2022YFA120470.

---

\* Corresponding author: pchenweis@gmail.com

- [1] L. Néel, *Science* **174**, 985 (1971).
- [2] L. Šmejkal, J. Sinova, and T. Jungwirth, *Phys. Rev. X* **12**, 031042 (2022).
- [3] L. Šmejkal, J. Sinova, and T. Jungwirth, *Phys. Rev. X* **12**, 040501 (2022).
- [4] I. Mazin (The PRX Editors), *Phys. Rev. X* **12**, 040002 (2022).
- [5] L. Šmejkal, A. B. Hellenes, R. González-Hernández, J. Sinova, and T. Jungwirth, *Phys. Rev. X* **12**, 011028

- (2022).
- [6] D.-F. Shao, S.-H. Zhang, M. Li, C.-B. Eom, and E. Y. Tsybal, *Nature Communications* **12**, 7061 (2021).
- [7] R. González-Hernández, L. Šmejkal, K. Výborný, Y. Yahagi, J. Sinova, T. c. v. Jungwirth, and J. Železný, *Phys. Rev. Lett.* **126**, 127701 (2021).
- [8] A. Bose, N. J. Schreiber, R. Jain, D.-F. Shao, H. P. Nair, J. Sun, X. S. Zhang, D. A. Muller, E. Y. Tsybal, D. G. Schlom, and D. C. Ralph, *Nature Electronics* **5**, 267 (2022).
- [9] N. Nagaosa, J. Sinova, S. Onoda, A. H. MacDonald, and N. P. Ong, *Rev. Mod. Phys.* **82**, 1539 (2010).
- [10] W. Feng, G.-Y. Guo, J. Zhou, Y. Yao, and Q. Niu, *Phys. Rev. B* **92**, 144426 (2015).
- [11] H. Bai, Y. C. Zhang, Y. J. Zhou, P. Chen, C. H. Wan, L. Han, W. X. Zhu, S. X. Liang, Y. C. Su, X. F. Han, F. Pan, and C. Song, *Phys. Rev. Lett.* **130**, 216701 (2023).
- [12] H. Bai, L. Han, X. Y. Feng, Y. J. Zhou, R. X. Su, Q. Wang, L. Y. Liao, W. X. Zhu, X. Z. Chen, F. Pan, X. L. Fan, and C. Song, *Phys. Rev. Lett.* **128**, 197202 (2022).
- [13] S. Karube, T. Tanaka, D. Sugawara, N. Kadoguchi, M. Kohda, and J. Nitta, *Phys. Rev. Lett.* **129**, 137201 (2022).
- [14] J. A. Ouassou, A. Brataas, and J. Linder, *Phys. Rev. Lett.* **131**, 076003 (2023).
- [15] C. Sun, A. Brataas, and J. Linder, *Phys. Rev. B* **108**, 054511 (2023).
- [16] Z. Savitsky, *Science* **383**, 574 (2024).
- [17] I. I. Mazin, *Phys. Rev. B* **107**, L100418 (2023).
- [18] P. E. Faria Junior, K. A. de Mare, K. Zollner, K.-h. Ahn, S. I. Erlingsson, M. van Schilfgaarde, and K. Výborný, *Phys. Rev. B* **107**, L100417 (2023).
- [19] L. Šmejkal, A. Marmodoro, K.-H. Ahn, R. González-Hernández, I. Turek, S. Mankovsky, H. Ebert, S. W. D'Souza, O. c. v. Šipr, J. Sinova, and T. c. v. Jungwirth, *Phys. Rev. Lett.* **131**, 256703 (2023).
- [20] M. Milivojević, M. Orozović, S. Picozzi, M. Gmitra, and S. Stavrić, *2D Materials* **11**, 035025 (2024).
- [21] T. Osumi, S. Souma, T. Aoyama, K. Yamauchi, A. Honma, K. Nakayama, T. Takahashi, K. Ohgushi, and T. Sato, *Phys. Rev. B* **109**, 115102 (2024).
- [22] Z. Lin, D. Chen, W. Lu, X. Liang, S. Feng, K. Yamagami, J. Osiecki, M. Leandersson, B. Thiagarajan, J. Liu, C. Felser, and J. Ma, *arXiv e-prints*, arXiv:2402.04995 (2024), arXiv:2402.04995 [cond-mat.mtrl-sci].
- [23] J. Krempaský, L. Šmejkal, S. D Souza, M. Hajlaoui, G. Springholz, K. Uhlířová, F. Alarab, P. Constantinou, V. Strocov, D. Usanov, *et al.*, *Nature* **626**, 517 (2024).
- [24] Y.-P. Zhu, X. Chen, X.-R. Liu, Y. Liu, P. Liu, H. Zha, G. Qu, C. Hong, J. Li, Z. Jiang, *et al.*, *Nature* **626**, 523 (2024).
- [25] M. Hiraiishi, H. Okabe, A. Koda, R. Kadono, T. Muroi, D. Hirai, and Z. Hiroi, *Phys. Rev. Lett.* **132**, 166702 (2024).
- [26] P. Keßler, L. Garcia-Gassull, A. Suter, T. Prokscha, Z. Salman, D. Khalyavin, P. Manuel, F. Orlandi, I. I. Mazin, R. Valentı, *et al.*, *arXiv preprint arXiv:2405.10820* (2024).
- [27] L. Onsager, *The London, Edinburgh, and Dublin Philosophical Magazine and Journal of Science* **43**, 1006 (1952).
- [28] A. Alexandradinata and L. Glazman, *Phys. Rev. B* **97**,

- 144422 (2018).
- [29] A. B. Pippard, “Magnetic breakdown,” in *Physics of Solids in Intense Magnetic Fields: Lectures presented at the First Chania Conference held at Chania, Crete, July 16–29, 1967*, edited by E. D. Haidemenakis (Springer US, Boston, MA, 1969) pp. 359–377.
- [30] See Supplemental Material at xxxx for the derivation of magnetic breakdown, general quantization condition, and Berry phase in the presence of spin-orbit coupling, which includes Refs. [3, 28, 37–39].
- [31] S. Shevchenko, S. Ashhab, and F. Nori, *Physics Reports* **492**, 1 (2010).
- [32] A. Alexandradinata and L. Glazman, *Annual Review of Condensed Matter Physics* **14**, 261 (2023).
- [33] M. Wubs, K. Saito, S. Kohler, Y. Kayanuma, and P. Hänggi, *New Journal of Physics* **7**, 218 (2005).
- [34] C. M. Wang, H.-Z. Lu, and S.-Q. Shen, *Phys. Rev. Lett.* **117**, 077201 (2016).
- [35] F. T. Vasko and O. E. Raichev, *Quantum Kinetic Theory and Applications: Electrons, Photons, Phonons* (Springer Science & Business Media, 2006).
- [36] R. Yu, W. Zhang, H.-J. Zhang, S.-C. Zhang, X. Dai, and Z. Fang, *science* **329**, 61 (2010).
- [37] T. E. O’Brien, M. Diez, and C. W. J. Beenakker, *Phys. Rev. Lett.* **116**, 236401 (2016).
- [38] S. N. Shevchenko, S. Ashhab, and F. Nori, *Physics Reports* **492**, 1 (2009).
- [39] I. S. Gradshteyn and I. M. Ryzhik, *Mathematics of Computation* **20**, 1157 C1160 (2007).